Liquid Lithium Divertor Characteristics and Plasma-Material Interactions in NSTX High-Performance Plasmas

M.A. Jaworski[1], T. Abrams[1], J.P. Allain[2], M.G. Bell[1], R.E. Bell[1], A. Diallo[1], T.K. Gray[3], S.P. Gerhardt[1], R. Kaita[1], J. Kallman[1,4], H.W. Kugel[1], B.P. LeBlanc[1], R. Maingi[3], A.G. McLean[4], J. Menard[1], R. Nygren[5], M. Ono[1], S.F. Paul[1], M. Podesta[1], A.L. Roquemore[1], S.A. Sabbagh[6], F. Scotti[1], C.H. Skinner[1], V.A. Soukhanovskii[4], D.P. Stotler[1], and the NSTX Team

[1]*Princeton Plasma Physics Laboratory, Princeton, NJ 08543, USA*
[2]*Purdue University, West Lafayette, IN 47907, USA*
[3]*Oak Ridge National Laboratory, Oak Ridge, TN 37831, USA*
[4]*Lawrence Livermore National Laboratory, Livermore, CA 94551, USA*
[5]*Sandia National Laboratory, Albuquerque, NM 87185, USA*
[6]*Columbia University, New York, NY 10027, USA*

E-mail contact of main author: mjaworsk@pppl.gov

Abstract. Liquid metal plasma facing components have been proposed as a means of solving several problems facing the creation of economically viable fusion power reactors. To date, few demonstrations exist of this approach in a diverted tokamak and we here provide an overview of such work on the National Spherical Torus Experiment (NSTX). The Liquid Lithium Divertor (LLD) was installed and operated for the 2010 run campaign using evaporated coatings as the filling method. The LLD consisted of a copper-backed structure with porous molybdenum front-face. Nominal Li filling levels by the end of the run campaign exceeded the porosity void fraction by 150%. Despite a nominal liquid level exceeding the capillary structure and peak current densities into the PFCs exceeding 100 [kA/m^2], no macroscopic ejection events were observed. In addition, no substrate line emission was observed indicating the lithium provides a protective coating on the molybdenum porous layer. Impurity emission from the divertor suggests that the plasma is interacting with oxygen-contaminated lithium whether diverted on the LLD or not. A database of LLD discharges is analyzed to consider whether there is a net effect on the discharges over the range of total deposited lithium in the machine. Examination of H-97L indicates that performance was constant throughout the run, consistent with the hypothesis that it is the quality of the surface layers of the lithium that impact performance. The accumulation of impurities suggests a fully-flowing liquid lithium system to obtain a steady-state PFC on timescales relevant to NSTX.

1. Introduction

Fusion reactors will eventually require a material from which to fabricate reactor components. To date, solid materials, most notably tungsten, has been the favored material for reactor studies. Tungsten plasma facing components (PFCs) are susceptible to several damage mechanisms in a reactor environment. The most significant of these are transient melting and deformation and the second is net erosion and redeposition due to sputtering and plasma transport processes. An alternative to solid PFCs are those whose plasma-facing surface is composed of a *liquid metal*. Candidate liquid metals include lithium, tin and gallium as well as some mixtures of those metals such as Sn-Li[1]. These PFCs have the potential to alleviate the aforementioned damage mechanisms in solid PFCs and could lead to more robust fusion reactors.

There have, to date, been few examples of liquid metal PFCs in fusion plasma experiments (CDX-U[2], FTU[3], T11-M[4], ISTTOK[5]) and none in a diverted configuration (though KTM[6] is beginning such development). Liquid metal PFCs include a set of technical challenges that require development before implementation into large machines. Lithium has been the favored metal for these studies (all previously mentioned machines except ISTTOK which uses gallium jets). The typical implementation previously has utilized a porous layer

in contact with a reservoir of liquid lithium. The liquid metal wicks into the porous layer and maintains a liquid metal surface facing the incident plasma[7]. This type of limiter has been used on CDX-U, FTU and T11-M. Alternative approaches are to utilize a pool of liquid metal as was done in the CDX-U experiment after experiments with the rail limiter[8]. While stable discharges were made on CDX-U, a similar sample cup geometry was tested in the DIII-D tokamak[9]. In this test an ELMy discharge resulted in macroscopic ejection of the lithium into the plasma exposing the substrate material (stainless steel or carbon). Plasma disruption followed after the ejection event. Stability of the liquid metal surface in the face of plasma heat and particle fluxes (both steady and transient) is of particular concern to the liquid metal approach.

The National Spherical Torus Experiment[10] (NSTX) has implemented a Liquid Lithium Divertor (LLD) module for experiments in the 2010 run campaign[11]. NSTX had previously utilized evaporated lithium onto graphite PFCs as a wall conditioning technique and demonstrated performance improvements[12,13,14]. The maintenance of lithium efficacy throughout an extended pulse (t_{pulse} > 1s) was a concern due to the known intercalation of lithium into graphitic materials[15]. A solid metal substrate was therefore considered to mitigate, if not eliminate, this process. In these proceedings we will describe the LLD as implemented in NSTX. The LLD did not exhibit macroscopic ejection of lithium from the surface and after liquefaction, no substrate impurities were observed from the surface[16]. Discharges on the LLD exhibited evidence of gettered impurities, however, which call into question the validity of these experiments as a test of a “pure” liquid lithium PFC surface.

2. Apparatus and Approach

A cross-section of the NSTX vessel is shown in Figure 1. The LLD was installed in the lower vessel at large major radius (0.65-0.85m in machine coordinates) where high-triangularity, high-performance discharges could be run on existing graphite PFCs and experiments could be conducted on the LLD surface in a single run campaign. The LLD consists of four 22cm wide plates each having a toroidal extent of 82.5°. The quadrants are separated toroidally by graphite tiles which contain diagnostics and other instrumentation. The LLD plates are made of 2.2cm thick copper with a 0.25mm stainless steel liner bonded to its surface. This stainless steel provides a barrier between lithium applied to the surface of the LLD and the copper substrate which would otherwise be chemically corroded by the lithium[17]. A flame-sprayed, porous molybdenum layer of approximately 0.15mm thickness forms the plasma-facing surface on top of the stainless steel layer. An image of the interior of NSTX is shown in figure 2 indicating the LLD position as installed prior to the run campaign.

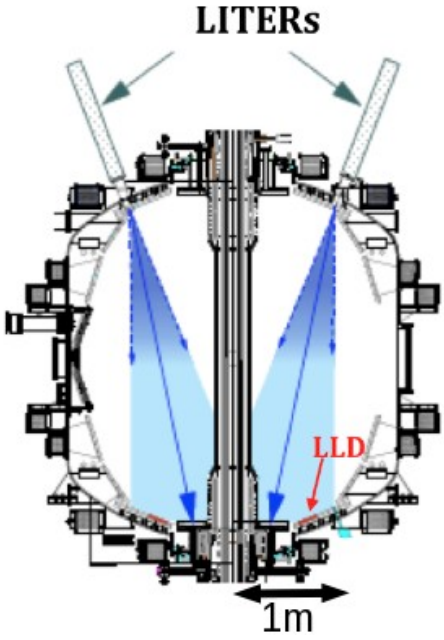

Figure 1: Cross-section of the NSTX vessel indicating location of the LLD installation in the lower vessel and LITER evaporation cones.

The LLD was intentionally installed to be slightly recessed of the adjacent graphite tiles. This was done to avoid any leading edges on the LLD itself which, by construction, only consisted of high-Z molybdenum on the front face whereas the side-walls consisted of a thin nickel plating over the stainless steel and copper bulk. The row of tiles inboard of

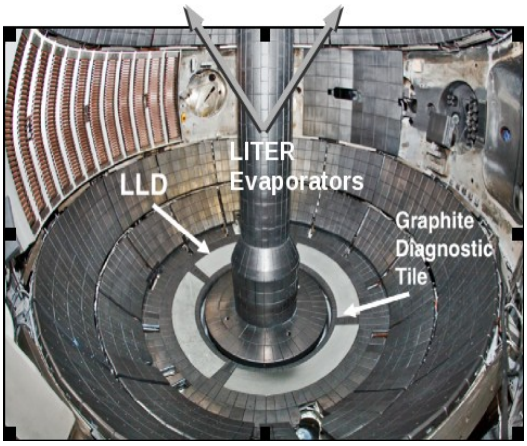

Figure 2: Image of the NSTX vessel interior. LLD plates are located in the lower portion of the vessel. Three of four inter-segment diagnostic breaks can also be seen. LITER evaporators are located at the vessel top as indicated in figure 1.

the LLD are referred to as the "bull-nose" tiles and extend from the LLD to the CHI-gap (62cm).

Porous molybdenum is used for several reasons. The first of which is to provide a low sputter-yield material to cover the stainless steel layer on the LLD. Additionally, moly compatible with liquid lithium over a wide range of foreseeable temperatures in NSTX whereas previous studies have shown lithium can corrode stainless steel[18]. Finally, the porous molybdenum facilitates the wetting and subsequent spreading of liquid lithium over the LLD and also insures that surface tension forces are large relative to electromagnetic forces to retain the liquid lithium during plasma operations[19].

The lithium capacity of the porous LLD surface was estimated to be 37g via image analysis of cross-sectional micrographs of the flame-sprayed material. The 2010 experiments were performed with the LLD filled with increasing amounts of deposited lithium, from a few percent at the beginning of the run campaign to an estimated 160% of fill on the last day of the run (60g). Each of the four LLD segments included embedded electrical heaters and thermocouples for monitoring heating. During operation, the thermocouples are disconnected immediately prior to a discharge and reconnected immediately following a discharge to avoid excessive currents to the heater control system. Due to this scheme, real-time thermocouple data is not available of the LLD segments, however a change in temperature from before and after the discharge can be calculated. As previously mentioned, the LLD was filled with lithium via the LITER evaporator system. Estimates place the filling efficiency of the LLD at about 7% of the total evaporated lithium[20]. Typical operation in NSTX makes use of between 100 and 700mg of lithium evaporated into the vessel over a 10-minute interval for about 90% of the discharges in a run campaign.

A new set of Langmuir probes in the High-Density Langmuir Probe array (HDLP) were also implemented in the 2010 campaign and are located in one of the inter-segment graphite diagnostic tiles. This probe array consists of 99 individual Langmuir probe tips arranged in a 3x33 pattern extending in radius from 62-72cm in machine coordinates. Only a subset of the 99 probes are instrumented at any one time, however the probes provide information on particle fluxes, plasma density and temperature of the plasma in their local vicinity. More information on the HDLP can be found in the literature[21,22,23]. The surface temperature of the LLD was monitored with the use of dual-band infrared thermography[24]. By using multiple infrared bands this system is capable of accounting for changes in emissivity of grey-body emitters and provide a more accurate surface temperature than a single-band system. Other diagnostics utilized include the typical suite a tools

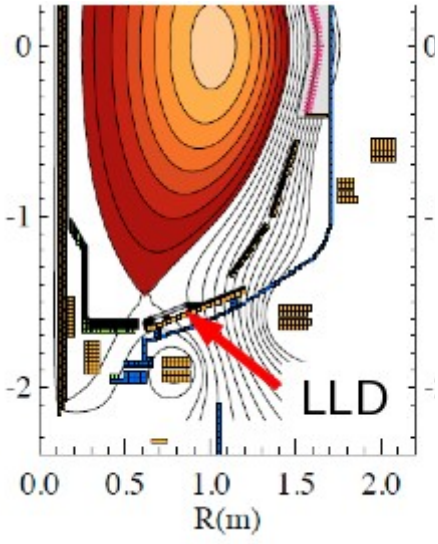

Figure 3: Typical equilibrium reconstruction for a discharge during LLD experiments. The outboard strike-point was located in the vicinity of the LLD or directly impinging it as in this example.

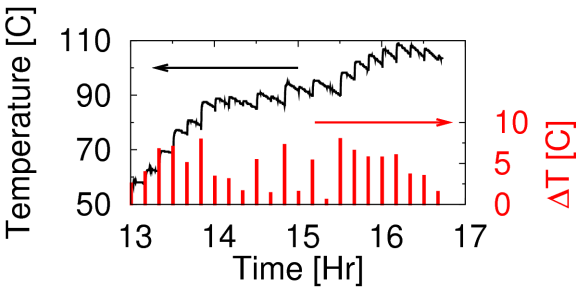

Figure 4: Example LLD temperature response during experiments. Mean temperature change for all four plates also shown. No active cooling was employed and resulted in a gradual rise in bulk temperature throughout the run day.

available on NSTX such as magnetic sensors (and associated EFIT reconstructions), divertor filter scopes and spectroscopy, and core measurements such as multi-point Thomson scattering and charge-exchange recombination spectroscopy.

During the 2010 NSTX experimental campaign, experiments dealing with the LLD itself were conducted over the course of the entire campaign at specific intervals. A typical plasma reconstruction is shown in figure 4. In these plasmas, a lower-single null discharge was formed with the outer strike point (OSP) near or impinging the LLD plates. When the OSP is not directly on the LLD, it is diverted onto the bull-nose tile immediately inboard of the LLD itself.

A database of the available discharges has been assembled in the following manner. As multiple diagnostics are available with disparate timebase signals, a single, uniform time-base signal is constructed from the selected diagnostics. This is done by obtaining a time-base signal and dividing the signal into uniform segments of 200ms in duration. The diagnostic signal is then averaged over the time-window to provide a typical value for this time in the discharge. An example is shown in figure 4. In some cases, spatial information is available in the underlying diagnostic, such as with multi-point Thomson and Langmuir probes in the divertor target. In these instances, the data are arranged on flux surfaces and a composite time-base signal is generated. Figure 4(d) shows such an example where multiple Langmuir probes fall within the range of $1.0<\Psi_N<1.005$, but a single time-trace can be produced from all the data falling within this window. This allows one to compare signals on similar magnetic surfaces from shot-to-shot. Figure 5 shows the temperature response of an LLD segment during a typical set of discharges. Each discharge deposits energy into the plate resulting in a temperature rise as indicated in the plot. The thermal insulation between the LLD segments is sufficient to use this temperature response for calorimetry. The energy rise of an LLD segment is given as $\Delta E=mc_p\Delta T$ where ΔE is the change in energy, m is the mass of the LLD plate, c_p is the specific heat of the copper and ΔT is the temperature rise. A mean heating power delivered to the plate by the plasma during the discharge can also be calculated using the pulse duration, τ_{pulse}, as $P_{LLD}=\Delta E/\tau_{pulse}$.

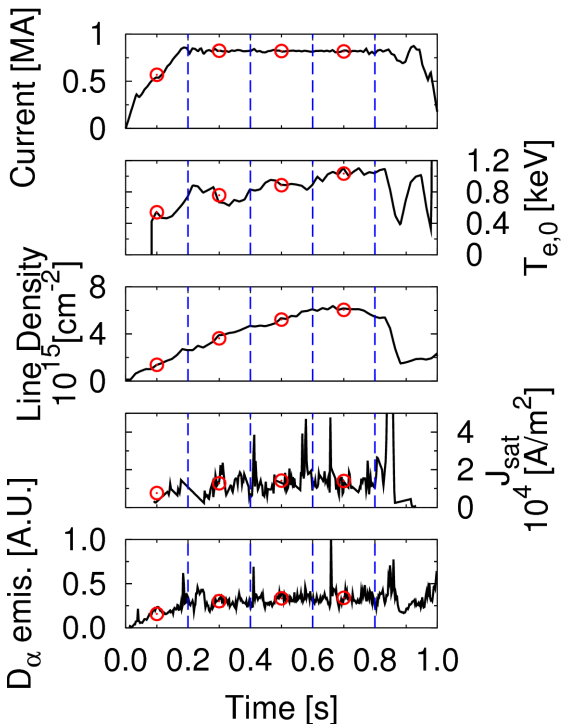

Figure 5: Example discharge (142521) showing full diagnostic signals (solid black line) and averaged values (red circles) within each time window (delineated by vertical lines).

3. Results and Discussion

The first notable results from operation with the LLD is that no molybdenum influx was observed during most discharges. As reported in ref. (16), early in the run, when evaporations had been performed on the LLD while cold,

molybdenum emission from the divertor was observed during MHD events. After reaching temperatures above the lithium melting point (181C), no such molybdenum emission was again observed. This repeats the results reported with the CPS devices which also indicated protection of the substrate material with liquid lithium PFCs[7].

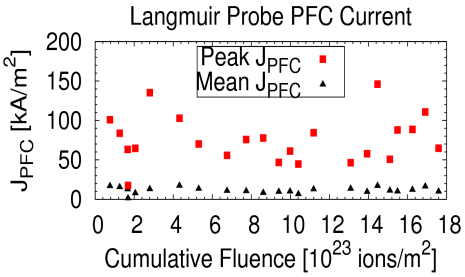

Figure 6: Quiescent and transient currents measured with the HDLP during a typical LLD run day. Each point represents an individual discharge where the mean current during the discharge is shown by the black triangles and the maximum value during transients is shown by the red squares.

The next notable result is that no macroscopic amounts of lithium were ejected from the LLD during the run campaign. Figure 6 shows a set of measurements of the current entering grounded PFCs during a typical run day as obtained with the HDLP. A typical quiescent current in the SOL of NSTX is at a level of 10 kA/m^2. Transiently, however, the currents entering the PFC can reach levels an order of magnitude above this. Using a variational principle, it is possible to derive a criteria for linear stability of a free-surface liquid metal under the action of body forces (electromagnetic and gravitational) taking into account surface tension forces and magnetic fields[19]. The stability criterion is given as follows:

$$n^2 = k\left(\frac{jB}{\rho - g}\right)\left[1 - \frac{k^2\Sigma}{(jB/\rho - g)\rho} - \frac{B^2 k_x^2}{2\pi\mu_0(jB/\rho - g)\rho k}\right]$$

where n is the growth rate (positive values of n are unstable, imaginary solutions are oscillatory only), k is the wave number of the perturbation, j is the current density, B the magnetic field intensity, ρ the density, g the acceleration due to gravity, Σ is the surface tension and μ_0 is the permeability of free space. We neglect viscous forces as these only slow the growth of an instability and do not affect whether the surface is unstable. The effect of the magnetic field is to dampen perturbations perpendicular to the field. This creates a favorable direction for instabilities in which the magnetic damping is negligible. The effect of the substrate geometry is to limit the wave numbers that can be present for this linear stability analysis. In these cases, the pore size of a porous layer enforces the radius and results in a stabilizing force. For these fastest-growing modes, then, the stability diagram for the NSTX and LLD is shown in figure 7. The regime of interest in NSTX is indicated, defined by the measured currents to the PFCs shown in figure 6 and the estimated pore size range. In the same figure, we make a comparison with results from the DIII-D Li-DIMES experiment which exhibited ejection of the lithium from a 25mm diameter, 1mm thick lithium sample whereas the pore diameter and film thickness on the LLD were of order 10-100 microns. The strategy of reducing pore size to stabilize a liquid metal was also implemented with the liquid lithium Capillary Porous System developed by Red Star[7]. In experiments in T11-M, it was found that by reducing the pore size of the mesh used in the CPS, droplet ejection could be eliminated. *This usage of a porous substrate for stabilization*

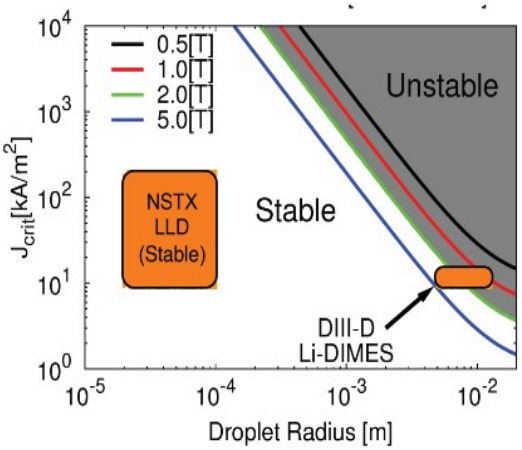

Figure 7: Stability diagram of for liquid metal under electro-magnetic body forces (with gravity and surface tension stabilizing). Comparison with Li-DIMES experimental space[9] also shown.

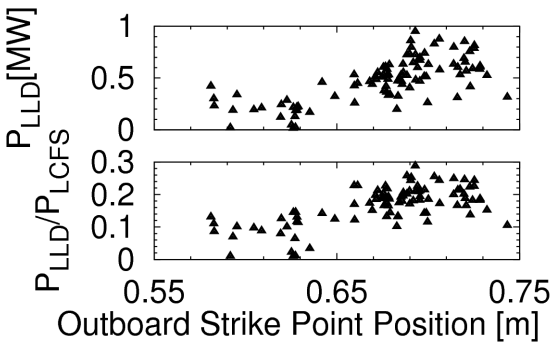

Figure 8: Mean heating power deposited in the lower divertor at the LLD location as determined by thermocouple calorimetry. Below, the same data as in (a) except as a fraction of the power crossing the LCFS. LLD nominal inner edge is at 0.65m.

of the free-surface liquid metal has now been demonstrated in a diverted tokamak.

The amount of power absorbed onto the LLD to depend on the strike point position. Figure 8 shows a comparison of absorbed power, as determined by calorimetry, as a function of strike point position. In fig. 8a the total absorbed power is shown and in fig. 8b, the fraction of power absorbed by the LLD of that crossing the last-closed flux surface (LCFS) is shown. For this shape of discharge and divertor flux expansion, probe analysis has indicated that the particle flux footprint is approximately 4-6cm. With this wide particle flux, a transition region between fully diverted onto the LLD and fully off the LLD could be expected between 65 and 70cm and this is indicated in the data. For these discharges, then, we can show that MW level heating powers were impinging the LLD and that approximately 25% of the power exiting the LCFS resulted in heating of the LLD when diverted onto it. IR thermography also indicates significant heat fluxes in the range of 2-10 MW/m^2 were typical of these discharges which is consistent with the estimated power density for a 4-6cm heating region. Post-mortem analysis of the LLD plates indicated that no failure of the copper-stainless steel-porous molybdenum structure had occurred despite the large heat fluxes (and associated thermal stresses) and electromagnetic forces acting on the plates. The LLD therefore demonstrates a liquid metal PFC at reactor-relevant heat-flux levels in the diverted configuration. This is consistent with laboratory experiments that also demonstrated protection of the substrate by lithium coatings and survival of 1.5 MW/m^2 heat fluxes[25].

Plasma diagnostics indicated that only subtle changes were occurring despite the change from carbon to molybdenum substrate. An examination of the divertor emission of several spectroscopic lines is shown in figure 9 as a function of the strike-point location. In transitioning to the LLD, a slight increase in the lithium and oxygen signals is observed as well as an increase in the probe J_{sat} in the near SOL. The probe fluxes are expected to be roughly proportional to the power crossing the LCFS if the electron temperature of the divertor is not changing to a large degree. This is, indeed, the case using the classical interpretation of the Langmuir probe signals[23] and both a Langmuir probe power

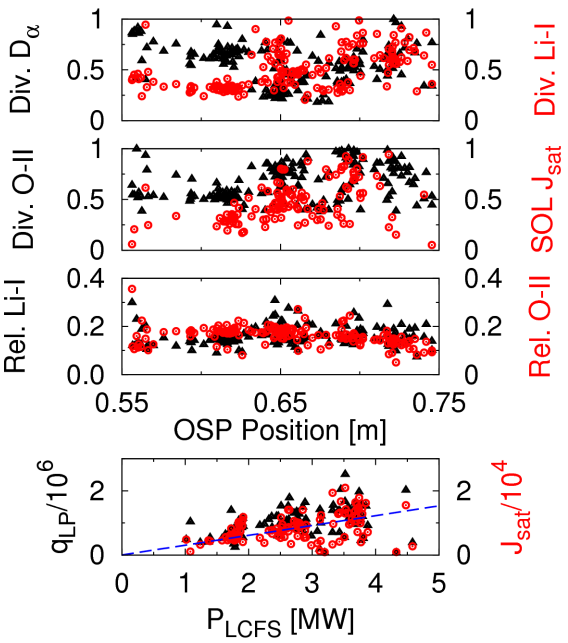

Figure 9: Divertor filterscope signals as a function of strike point radius (0.4-0.6s). Figures (a) and (b) show the relative emission for D-alpha, Li-I, and O-II lines as well as the Langmuir probe J_{sat} for the region $1.0<\Psi_N<1.005$. Data in figures (a) and (b) are normalized to 1 to emphasize any qualitative structure in the data. Flux (heat or particle) are shown to be roughly proportional to the exhaust power in the machine in (d). Linear least-squares fit of *f(x)=ax* shown. Relative emission of Li-I or O-II normalized to exhaust power vs. strike point position in (d).

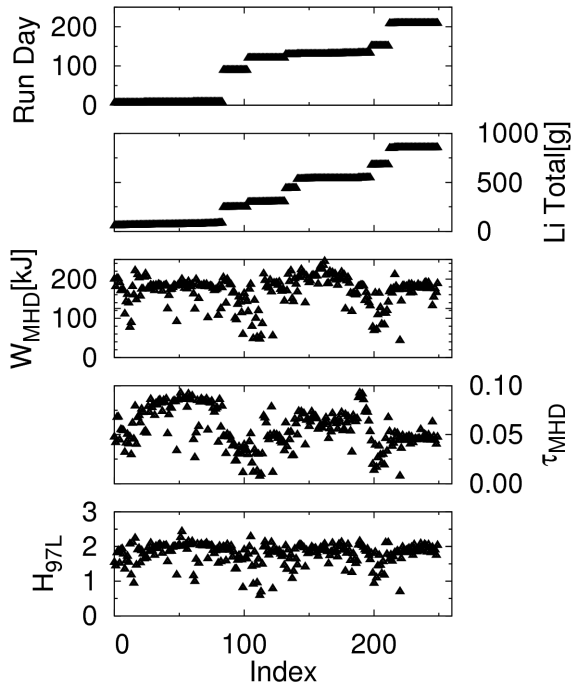

Figure 10: Selected entries from the LLD experimental database. Run day is the number of days since the beginning of the experimental campaign, Li Total is the integrated amount of lithium evaporated into the vessel, W_{MHD} is the plasma stored energy, τ_{MHD} is the energy confinement time, H-97L is the H-factor compared to the ITER 97L global confinement scaling[28]. W_{MHD}, τ_{MHD} and H-97L taken as the average between 400-600ms.

flux or J_{sat} are roughly proportional to P_{LCFS}. One can the normalize the divertor emission signals to remove bias due to increased P_{LCFS} or J_{sat} and replot the data in figures 8(a) and (b) and this is shown in figure 8(d). One can see in the data that very little difference is now present in those discharges diverted over the LLD or onto the graphite bull-nose tiles.

Oxygen is a prevalent contaminant in lithium experiments. In the PISCES-B linear plasma device, extensive plasma cleaning was required to remove the oxygen[26]. In addition, laboratory tests have shown that in the presence of 1e-6 partial pressures of water vapor, oxygen-containing surface layers will form in about 10s[27]. Intershot pressure in the NSTX vacuum vessel is of order 1e-7 Torr and the intershot time is about 600s, providing ample time for surface oxygen layers to form. The slow filling process by evaporation in NSTX is therefore prone to contamination by background gases and reduces the likelihood that any LLD discharges could be considered a fair test of a "pure" liquid lithium PFC.

Further indication of this is seen in the behavior of confinement time over the entire set of LLD discharges for the year. We show in figure 10 a summary of the database for a set of selected entries. Experiments were largely conducted in three groups at the beginning, middle and end of the campaign with a large variance in the amount of total lithium in the machine. A cursory look at a calculated confinement time from equilibrium reconstructions might lead one to consider performance to have decreased. However, normalizing against ITER97 L-mode scaling[28] indicates that performance at the beginning of the run was nearly identical with that at the beginning of the run campaign. If the relevant quality of the lithium in the machine is determined by the *contamination rate of the lithium surface*, which is much shorter than the inter-discharge timescale, then one would expect large quantities of evaporated lithium not to significantly alter the machine performance and this is consistent with the data from the FY2010 run campaign.

4. Conclusions and future work

The NSTX LLD campaign has resulted in several important results related to the implementation of liquid metal PFCs. First, the LLD confirmed the result on limiter machines that liquid lithium provides a protective layer over a high-Z metal substrate. Next, the LLD demonstrated a stable liquid metal using a porous substrate for the first time in a diverted tokamak. In addition to the liquid metal stability, the overall construction of a porous metal substrate was able to successfully operate the entire run year without evidence of damage during post-mortem analysis. Finally, there are indications that the plasma response over the LLD is not distinguishable from plasmas diverted over the graphite tiles immediately adjacent. This is consistent with a nearly constant H-factor throughout the run campaign. Further, laboratory studies indicate that oxygen-containing impurity layers form

on comparable (if not shorter) timescales as a typical NSTX shot sequence. The hypothesis that it is the *quality of the lithium surface* that impacts plasma performance is consistent with the observed independence of confinement vs. the total quantity of lithium in the machine.

The need to mitigate the accumulation of impurities on the surface of the lithium PFCs is strongly suggested by this data set. A fully flowing liquid lithium divertor would provide a means of removing impurities continuously from the surface and bulk of the lithium in the vessel. In addition, bulk cleaning of lithium has been demonstrated on PISCES-B[26] and may be possible with longer pulse-lengths in the NSTX-U. Development is underway for a fully-flowing system in the long-range planning of NSTX-U while near-term experiments examining local transport of lithium and its impurities is underway in the laboratory and on linear test-stands.

Acknowledgments

This work supported by USDOE contracts DE-AC02-09CH11466, DE-AC05-00OR22725, DE-AC52_07NA27344, DE-FG02-99ER54524, DE-FG02-08ER54990 and DE-AC04-94AL85000.

References

[1] M. Abdou, et al., Fusion Eng. Des. **54** (2001) 181-247.
[2] R. Majeski, et al., J. Nucl. Mater. **313-316** (2003) 625-629.
[3] G. Mazzitelli, et al., Nucl. Fusion **51** (2011) 073006.
[4] S.V. Mirnov and V.B. Lazarev, J. Nucl. Mater. **415** (2011) S417-S420.
[5] R.B. Gomes, et al., J. Nucl. Mater. **415** (2011) S989-S992.
[6] I. Tazhibayeva, et al., Proc. 22nd IAEA Fusion Energy Conf. FTP/P6-08.
[7] V.A. Evtikhin, et al., J. Nucl. Mater. **307-311** (2002) 1664-1669.
[8] R. Kaita, et al., Phys. Plasmas **14** (2007) 056111.
[9] D.G. Whyte, et al., Fusion Eng. Des. **72** (2004) 133-147.
[10] M. Ono, et al., Nucl. Fusion **40** (2000) 557.
[11] H.W. Kugel, et al., Fusion Eng. Des. *In press*.
[12] M.G. Bell, et al., Plasma Phys. Control. Fusion **51** (2009) 124054.
[13] R. Maingi, et al., Nucl. Fusion **52** (2012) 083001.
[14] S.M. Kaye, et al., Proc. 24th IAEA Fusion Energy Conf. San Diego, CA, Oct. 8-13, 2012 EX/7_1(2012).
[15] N. Itou, et al., J. Nucl. Mater. **290-293** (2001) 281-285.
[16] V.A. Soukhanovskii, et al., Rev. Sci. Instrum. **81** (2010) 10D723.
[17] "Liquid-metals handbook", United States Office of Naval Research. U.S. Govt. Print. Off. 1950.
[18] H. Katsuta, et al., J. Nucl. Mater. **71** (1977) 95-104.
[19] M.A. Jaworski, et al., J. Nucl. Mater. **415** (2011) S985-S988.
[20] H.W. Kugel, et al., Fusion Eng. Des. **85** (2010) 865-873.
[21] J. Kallman, et al., Rev. Sci. Instrum. **81** (2010) 10E117.
[22] M.A. Jaworski, et al., Rev. Sci. Instrum. **81** (2010) 10E130.
[23] M.A. Jaworski, et al., Fusion Eng. Des. (2012) *in press.*
[24] A.G. McLean, et al., Rev. Sci. Instrum. **83** (2012) 053706.
[25] T. Abrams, et al., J. Nucl. Mater. *Submitted.*
[26] R. Doerner, et al., J. Nucl. Mater. **290-293** (2001) 166-172.
[27] C.Skinner, et al., J. Nucl. Mater. *Submitted*.
[28] S.M. Kaye, et al., Nucl. Fusion **37** (1997) 1303-1328.